Earth and Planetary Science Letters 547 (2020) 116438

Contents lists available at ScienceDirect

Earth and Planetary Science Letters

www.elsevier.com/locate/epsl

Deformation across the mantle transition zone: A theoretical mineral physics view

Sebastian Ritterbex [a,b,*], Philippe Carrez [a], Patrick Cordier [a,c]

[a] Univ. Lille, CNRS, INRAE, Centrale Lille, UMR 8207 - UMET - Unité Matériaux et Transformations, F-59000 Lille, France
[b] Geodynamics Research Center, Ehime University, 2-5 Bunkyo-cho, Matsuyama 790-8577, Japan
[c] Institut Universitaire de France, 1 rue Descartes, 75005 Paris, France

ARTICLE INFO

Article history:
Received 28 October 2019
Received in revised form 1 June 2020
Accepted 23 June 2020
Available online xxxx
Editor: J. Brodholt

Keywords:
deformation modeling
transition zone
pure climb creep
wadsleyite
ringwoodite
majorite

ABSTRACT

The dynamics of the Earth's mantle is still poorly constrained due to the lack of understanding the transfer of matter between the upper and the lower mantle and their convective vigor. The transition zone (TZ) might play a crucial role as the interface connecting the upper to the lower mantle. Here, we examine the rheology of the main TZ minerals, wadsleyite, ringwoodite and majorite garnet based on a mineral physics approach. Using the results of lattice friction modeling and dislocation glide mobilities together with the available data on self-diffusion in the TZ minerals, we quantify their plastic deformation by diffusion and dislocation creep from theoretical plasticity models. We show that pure climb creep is expected to contribute to the plasticity of the TZ without the need of significant diffusion-related hydrolytic weakening, matching well the geophysical observations. Our model results predict that crystallographic preferred orientations (CPO) might only develop along with stress concentrations as present around cold subducting slabs which can be locally weaker than the surrounding TZ despite their lower temperatures.

1. Introduction

The mantle transition zone (TZ), extending between 410 and 660 km depth, influences the dynamics of the Earth's interior as it accommodates the transfer of matter between the upper and the lower mantle by subducting slabs and upwelling plumes. Seismic tomography reveals that some slabs penetrate through the TZ while others stagnate either within or just below at a depth of ~1000 km (van der Hilst et al., 1991; Fukao et al., 2001; Grand, 2002; Zhao, 2004; Fukao and Obayashi, 2013). Likewise, plumes imaged in the lower mantle appear as large columnar structures with diameters up to ~1000 km, while their signature changes drastically across the TZ into the upper mantle (French and Romanowicz, 2015). These tomographic features provide evidence for whole mantle convection, but they also suggest a change in the dynamics of the mantle to occur across the TZ, implying different styles of convection between the upper and lower mantle. Moreover, while the first ~300 km of the upper mantle exhibit strong seismic anisotropy (e.g. Fischer and Wiens, 1996; Long and van der Hilst, 2006), it remains comparably small throughout most of the transition zone, and is particularly localized in the vicinity of subducting slabs with fast SV anomalies up to ~3% (Drilleau et al., 2013; Moulik and Ekström, 2014; Lynner and Long, 2015; Huang et al., 2019; Ferreira et al., 2019; Chang and Ferreira, 2019). This supports the idea that the dynamics across the TZ might be driven by a different rheology than that of the upper mantle, since the presence or absence of global seismic anisotropy might be related to the active creep mechanisms governing solid-state flow in the mantle (Mainprice, 2007; Karato et al., 2008; Boioli et al., 2017). Therefore, understanding the differences in the mechanical properties between the upper and lower mantle across the TZ is needed to put better constraints on the dynamics of the Earth's interior. However, the rheology of the TZ remains poorly understood.

The TZ is characterized by a number of pressure-induced phase transitions, from olivine to wadsleyite at ~410 km depth, wadsleyite to ringwoodite at ~520 km depth, and ringwoodite and majorite garnet to bridgmanite and ferropericlase at ~660 km depth (Ringwood, 1975). Wadsleyite and ringwoodite constitute the main volumetric fraction (up to ~60%) of the TZ, while the remaining ~40% consists of majorite garnet (Ita and Stixrude, 1992). Most recent high pressure (P) and temperature (T) deformation experi-

* Corresponding author at: Geodynamics Research Center, Ehime University, 2-5 Bunkyo-cho, Matsuyama, Ehime 790-8577, Japan.
E-mail address: ritterbex.sebastian_arthur_willem.us@ehime-u.ac.jp (S. Ritterbex).

https://doi.org/10.1016/j.epsl.2020.116438
0012-821X/

ments of the high-P polymorphs of olivine (Nishihara et al., 2008; Farla et al., 2015; Hustoft et al., 2013; Kawazoe et al., 2010, 2013; Meade and Jeanloz, 1990; Kavner and Duffy, 2001; Nishiyama et al., 2005; Miyagi et al., 2014) reveal high flow stresses during quasi steady state deformation at typical laboratory strain rates of $\sim 10^{-5}$ s^{-1}. It was demonstrated that the flow stress under quasi steady state conditions for both wadsleyite and ringwoodite remains generally ~2-4 GPa at the appropriate P, T conditions of the TZ. Recent theoretical modeling of the lattice friction of slip systems and high-P and high-T dislocation glide in Mg_2SiO_4 wadsleyite (Ritterbex et al., 2016) and ringwoodite (Ritterbex et al., 2015) confirmed these experimental results and showed that dislocation glide is expected to control their mechanical behavior at laboratory conditions. These theoretical studies are based on a non-empirical approach to derive the glide velocity of dislocations in the high-P polymorphs of olivine at the relevant P, T conditions of the TZ and provide evidence of substantial lattice friction, inhibiting dislocation glide if deformation occurs at very low strain rates of the mantle. Although dislocation mobilities in majorite garnet have not been modeled yet, non-hydrostatic compression experiments reveal a significant mechanical strength of majorite (Kavner et al., 2000), comparable to that of wadsleyite and ringwoodite, in fair agreement with previous predictions of Karato et al. (1995). Despite substantial lattice resistance of TZ minerals at laboratory conditions, their plasticity can be promoted by atomic diffusion at mantle temperatures and low strain rates allowing dislocations (Martin and Caillard, 2003). Besides dislocation creep, the TZ constituents might as well deform efficiently by grain size sensitive diffusion creep, particularly if grains are small. Deformation within the diffusion creep regime is thus important to consider in the TZ where many phase transitions occur and heterogeneities as slabs and plumes are present. Therefore, atomic diffusivities of the TZ constituents play a key role in modeling their plastic deformation. Here, we use the available data of diffusion and dislocation glide in the high-P polymorphs of olivine and majorite garnet and quantify the plastic contributions of both diffusion and dislocation creep based on theoretical plasticity models. The results put constraints on the rheology of the TZ and its implications to the dynamics of the mantle will be briefly discussed.

2. Modeling the mechanisms of plastic deformation

2.1. Atomic diffusivity

Point defect diffusion is one of the rate-limiting steps controlling deformation mechanisms of minerals at high homologous temperature in the Earth's mantle (Poirier, 1985). Plastic deformation in the mantle TZ is thus expected to be strongly constrained by the diffusivity of its main constituents. Fig. 1 presents all self-diffusion data available from high-P, T experiments on wadsleyite, ringwoodite and majorite garnet (Shimojuku et al., 2004, 2009, 2010; Zhang et al., 2011; Holzapfel et al., 2009; van Mierlo et al., 2013). The Fe-Mg interdiffusion data from these studies are not shown as they are much larger than the Si and O self-diffusion coefficients. These experimental data (Fig. 1) suggest that Si is the slowest diffusing species in wadsleyite and ringwoodite and is therefore expected to control the overall rate of atomic diffusion. Moreover, these experiments (Fig. 1) show a striking similarity (within one order of magnitude) between the Si diffusivities in wadsleyite and ringwoodite and the self-diffusion coefficient of $MgSiO_3$ majorite garnet between ~1600-2000 K, despite the variations in starting materials between experiments. Being the result of different experimental conditions (e.g. oxygen fugacity, impurity content, etc.), potentially influencing the point defect concentrations and mobilities, these data provide strong evidence that the rate limiting diffusivity of wadsleyite, ringwoodite and majorite are

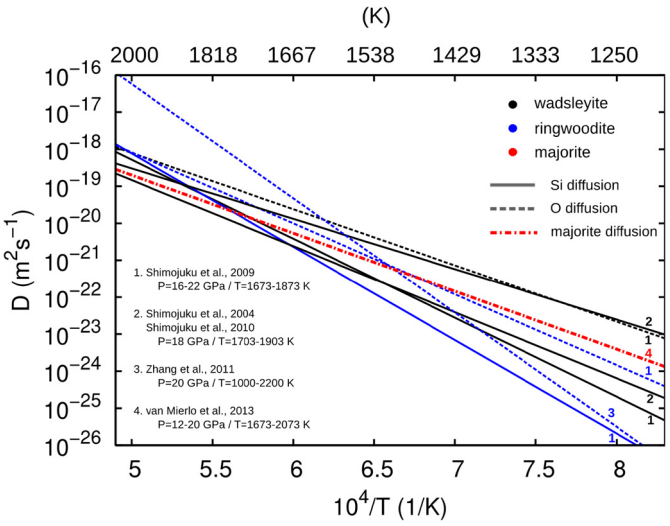

Fig. 1. Arrhenius plot of the self-diffusion coefficients D_{sd} in wadsleyite, ringwoodite and majorite garnet. Colors indicate different minerals. Different atomic diffusion species are indicated by different line characters. (For interpretation of the references to color in this figure, the reader is referred to the web version of this article.)

comparable without much variation under the appropriate P, T conditions of the TZ.

2.2. Diffusion creep

The deformation mechanisms responsible for plastic strain resulting from pure atomic diffusion are commonly referred to as diffusion creep (Poirier, 1985). Diffusion creep is a grain size sensitive deformation mechanism which is particularly activated when grain boundaries are the main sources and sinks of point defect (e.g. in fine grained materials). Diffusion creep corresponding to diffusional transport through the bulk of grains is commonly known as Nabarro-Herring creep (NHC) and is described as (Nabarro, 1948; Herring, 1950)

$$\dot{\varepsilon}_{NH} = A_{NH} \frac{D_{sd} \sigma \Omega}{d^2 k_b T}, \tag{1}$$

where d is the mean grain size, $\dot{\varepsilon}$ the strain rate, σ the flow stress, D_{sd} the bulk diffusion coefficient, Ω the activation volume for diffusion, k_b the Boltzmann constant, and A_{NH} a shape factor frequently considered as 16/3, corresponding to a spherical geometry of grains and the impossibility of grain boundary sliding (Poirier, 1985). Another variant of diffusion creep is Coble creep (CC), a mechanism where plastic deformation is due to diffusional transport along grain boundaries, which is described as (Coble, 1963)

$$\dot{\varepsilon}_{NH} = A_C \frac{D_{gb} \delta \sigma \Omega}{d^3 k_b T}, \tag{2}$$

where D_{gb} is the grain boundary diffusion coefficient and δ the grain boundary thickness. From Eqs. (1) and (2), it can be seen that the diffusion creep mechanisms become particularly efficient in fine grained materials. A transition from NHC to CC can be expected with decreasing grain size.

2.3. Dislocation creep

Dislocation creep is a grain size insensitive intracrystalline deformation mechanism responsible for the transport of shear through the crystalline lattice, mediated by linear crystal defects called dislocations, along some specific directions and planes. Dislocation creep is a composite deformation mechanism that may

involve both glide and climb processes. Based on the plasticity of metals, Weertman (1957) proposed a theoretical dislocation creep model relying on the ratio of the glide (v_g) and climb (v_c) velocities of dislocations. In most metals at $T > 0.4T_m$, the ratio $v_g/v_c \gg 1$ so that plastic strain is efficiently produced by dislocation glide, whereas the climb velocity controls the rate of deformation. Indeed, dislocation dynamics simulations (DD) of Al have shown that the activation of climb allows to bypass obstacles and to recover dislocation junctions efficiently allowing strain to be produced by dislocation glide (Keralavarma et al., 2012; Danas and Deshpande, 2013; Huang et al., 2014). More recently, DD simulations of Boioli et al. (2015a) on Mg_2SiO_4 olivine, for which $v_g/v_c \gg 1$ at P, T and low stress conditions of the upper mantle, predicted that its plasticity is governed by Weertman creep, described by a usual power-law equation with a stress exponent $n = 3$ in analogy with the empirically deduced equation for high-T creep of olivine (Hirth and Kohlstedt, 2003).

In contrast to olivine, Boioli et al. (2017) predicted that $v_g/v_c \ll 1$ in Mg_2SiO_4 ringwoodite at TZ P, T and low mantle stresses. These results were obtained in the framework of DD, where the climb velocities of dislocations with a cylindrical geometry are solved under steady state conditions from the diffusion equation as (Boioli et al., 2015b)

$$v_c = \frac{2\pi}{\ln(1/2\sqrt{\rho_t})}\frac{D_{sd}}{b}\left[\exp\left(\frac{\sigma\Omega}{k_bT}\right) - 1\right] \tag{3}$$

where b is the magnitude of the Burgers vector, and $\rho_t = (\sigma/\mu b)^2$ the total dislocation density at low stress σ, based on the line tension, and μ the shear modulus. On the other hand, theoretical modeling of thermally activated processes responsible for dislocation glide have predicted dislocation glide velocities in Mg_2SiO_4 wadsleyite (Ritterbex et al., 2016) and ringwoodite (Ritterbex et al., 2015). These theoretical results were previously compared with the available data from deformation experiments of wadsleyite and ringwoodite, demonstrating that the contribution of dislocation glide during plastic deformation is able to reproduce the high stress levels required to deform wadsleyite and ringwoodite at high-P and high-T of the transition zone and experimental deformation rates. Even though other elementary creep processes might contribute to the overall plasticity of wadsleyite and ringwoodite, this remarkable agreement suggests that dislocation glide is expected to be a controlling factor in the mechanical behavior of the high-P polymorphs of olivine at laboratory conditions, supported by TEM observations of deformed samples (Ritterbex et al., 2016; Nzogang et al., 2018). These previous results show that high lattice friction opposing to dislocation glide in wadsleyite and ringwoodite is responsible for the high stress levels observed during experimental deformation which are predicted to remain substantially high even at the very low strain rates corresponding to the deformation conditions of the Earth's mantle. In these previous studies, the average glide velocity v_g is determined as a function of P, T via the stress dependence of the nucleation rate of kink-pairs as

$$v_g = b\frac{L}{l_c}\nu_D\frac{b}{l_c}\exp\left(-\Delta H_c(\sigma)/k_bT\right) \tag{4}$$

where ΔH_c is the enthalpy associated with kink-pair nucleation at the dislocation line, $L = 1/\sqrt{\rho_t}$ the line length of dislocations, ν_D the Debye frequency and l_c the critical kink-pair length. Using Eqs. (3) and (4), we revisit and extend the previous work of Boioli et al. (2017) and determine the ratio v_g/v_c of dislocations belonging to the easiest slip systems in both high-P polymorphs of Mg_2SiO_4 olivine. The parameters b, μ, l_c and ΔH_c are taken from previous theoretical work (Ritterbex et al., 2015, 2016). The self-diffusion coefficients of wadsleyite and ringwoodite are parameterized by the diffusivity of Si as the slowest diffusing species (Fig. 1) from experimental results (Shimojuku et al., 2010, 2009). We further assume a ρ_t cutoff of 10^{14} m^{-2} since ρ_t becomes stress independent at high values (Boioli et al., 2015b). Results of v_g/v_c as a function of P, T and stress are presented in Fig. 2. Below stresses of ~0.5 GPa and ~1.2 GPa, $v_g < v_c$ for wadsleyite and ringwoodite, respectively. Particularly at mantle stresses (~1 MPa) Weertman creep appears to become impossible and dislocation climb turns into a potential strain-producing mechanism, in contrast to olivine at upper mantle conditions (Boioli et al., 2015a). This provides evidence that a transition in deformation mechanism in the dislocation creep regime can be expected at low stresses (Fig. 2). Below this transition stress, the strain producing climb process is expected to control the rate of deformation. The latter is similar to the situation of bridgmanite (Boioli et al., 2017; Reali et al., 2019), where DD simulations demonstrated that steady state creep could be achieved through plastic shear by the exchange of point defects between dislocations, a deformation mechanism known as pure climb creep (PCC) which was first predicted by Nabarro (1967). It can thus be expected that dislocation creep in wadsleyite and ringwoodite at TZ conditions is promoted by PCC, where dislocations are the sources and sinks of point defects. The strain rate produced by this mechanism is analytically derived as (Nabarro, 1967)

$$\dot{\varepsilon}_n = \frac{1}{\pi\ln(\frac{4\mu}{\pi\sigma})}\frac{D_{sd}\mu b}{k_bT}\left(\frac{\sigma}{\mu}\right)^3 \tag{5}$$

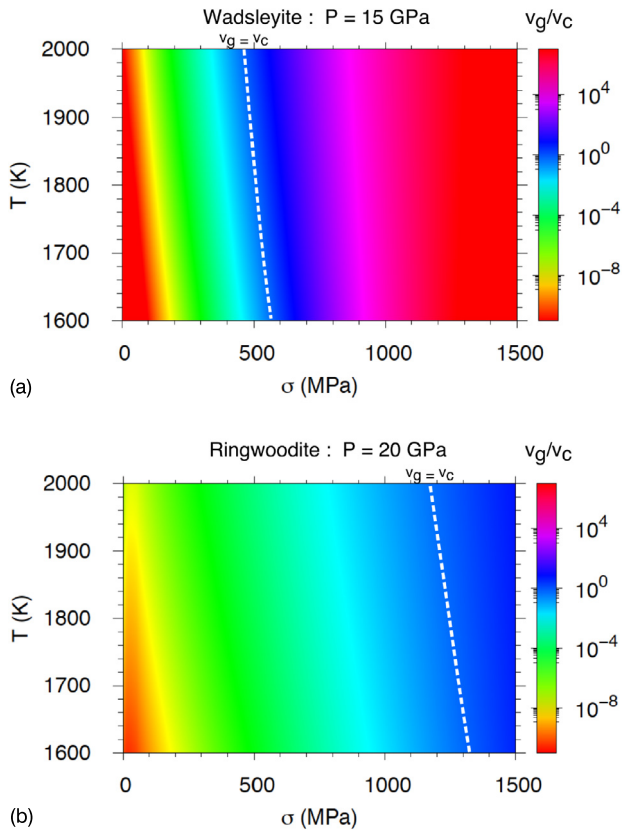

Fig. 2. Ratio of the glide (v_g) versus climb velocities (v_g) of dislocations as a function of the flow stress σ and temperature T. a) The easiest 1/2<111>{101} slip system in wadsleyite at 15 GPa. b) The easiest 1/2<110>{110} slip system in ringwoodite at 20 GPa.

Table 1
Experimental data of bulk self-diffusion coefficients $D_{sd} = D_0 \exp(-E/RT)$ of wadsleyite, ringwoodite and majorite garnet.

Phase	P (GPa)	T (K)	Diffusing specie	D_0 ($m^2\ s^{-1}$)	E (kJ/mol)
Wadsleyite (Shimojuku et al., 2004)	18	1703-1903	Si	$2.00 \cdot 10^{-12}$	261
Wadsleyite (Shimojuku et al., 2009)	16	1673-1873	Si	$2.51 \cdot 10^{-8}$	409
Wadsleyite (Shimojuku et al., 2010)	18	1673-1873	Si	$1.26 \cdot 10^{-10}$	342
Ringwoodite (Shimojuku et al., 2009)	22	1673-1873	Si	$3.16 \cdot 10^{-6}$	483
Majorite garnet (van Mierlo et al., 2013)	18	1673-2073	$MgSiO_3$	$1.4 \cdot 10^{-11}$	295

Table 2
Experimental data of grain boundary self-diffusion coefficients $\delta D_{gb} = \delta D_0 \exp(-E/RT)$ of wadsleyite and ringwoodite.

Phase	P (GPa)	T (K)	Atomic specie	δD_0 ($m^3\ s^{-1}$)	E (kJ/mol)
Wadsleyite (Shimojuku et al., 2004)	18	1703-1903	Si	$1.58 \cdot 10^{-17}$	257
Wadsleyite (Shimojuku et al., 2009)	16	1673-1873	Si	$1.26 \cdot 10^{-15}$	327
Wadsleyite (Shimojuku et al., 2010)	18	1673-1873	Si	$1.00 \cdot 10^{-20}$	159
Ringwoodite (Shimojuku et al., 2009)	22	1673-1873	Si	$6.31 \cdot 10^{-14}$	402

where the dislocation microstructure results from the balance between dislocation multiplication by the activation of Bardeen-Herring sources (Bardeen and Herring, 1952) and dipole annihilation. This implies that the PCC regime is limited to operate in grains with a minimum size for a given stress σ, since the opening of a Bardeen-Herring source from line tension requires that $\sigma = \mu b/l_s$, where l_s is the critical source length which has to be smaller than the size of the crystal (Knight and Burton, 1989; Mordehai et al., 2008). It is worth to mention that in absence of the glide process, this mechanism which does not involve simple shear, is unable to induce lattice rotation and no CPO can be formed during plasticity, in contrast to Weertman creep.

3. Results: deformation mechanisms maps

3.1. Wadsleyite and ringwoodite

The available data of bulk (Table 1) and grain boundary (Table 2) self-diffusion in wadsleyite and ringwoodite are used to construct deformation mechanism maps including NHC (Eq. (1)), CC (Eq. (2)) and PCC (Eq. (5)). These maps allow to compare the relative efficiency through which plastic strain is produced by these mechanisms. The activation volumes for diffusion Ω, equal to the unit cell volume per number of formula units, are taken from first-principles quasi-harmonic calculations at the P, T conditions of the TZ (Wentzcovitch et al., 2010; Yu et al., 2011). The shear moduli μ of wadsleyite and ringwoodite at TZ P, T conditions are estimated as a function of depth from the Preliminary Reference Earth Model (PREM) (Dziewonski and Anderson, 1981). The magnitudes of the Burgers vectors b have been considered for dislocations belonging to the easiest slip systems: 1/2<111>{101} in wadsleyite (Ritterbex et al., 2016) and 1/2<110>{110} in ringwoodite (Ritterbex et al., 2015). Deformation mechanism maps are built by solving Eq. (1), (2) and (5) for a fixed steady state strain rate and T. Both variations in strain rate and T are considered. The dominant deformation mechanism is defined as the lowest flow stress required at a fixed steady-state strain rate. Figs. 3 and 4 represent the deformation mechanism maps for wadsleyite at 15 GPa and ringwoodite at 20 GPa, respectively. Black points mark the transition between the deformation mechanisms. CC dominates for a grain size interval in the red area, NHC in the blue area and PCC in the grey area. Different curves per deformation mechanism correspond to the different Si bulk and grain boundary diffusivities available from previous studies, summarized in Tables 1 and 2. PCC is represented as a horizontal line since this mechanism is grain size independent, but is only allowed to operate in grains larger than a critical length l_s which ensures the opening of a Bardeen-Herring source. For strain rates between 10^{-14} and 10^{-17} s^{-1} and T between 1500-1800 K in wadsleyite and 1700-2000 K in ringwoodite, PCC becomes dominant when grains are larger than ~0.2-4 mm. At the same time, the results for PCC represent an upper bound for the viscosity, varying between $\sim 10^{20}$ Pa.s and a maximum of $\sim 10^{22}$ Pa.s. If grains are smaller than ~1 mm, diffusion creep becomes increasingly more dominant, leading to substantially lower viscosities. A strong similarity is found between the deformation mechanism maps of wadsleyite and ringwoodite, in particular in the pure climb creep regime, since creep is mainly rate-controlled by comparable Si diffusivities (Fig. 1).

3.2. The case of majorite garnet

Dislocation glide in $MgSiO_3$ majorite garnet has not been theoretically investigated, and the glide versus climb mobilities cannot be determined. Nevertheless, *ex-situ* transmission electron microscopy (TEM) characterization of dislocation microstructures in majorite garnet during high-P, T deformation in the multi-anvil apparatus provides evidence of substantial lattice friction (Couvy et al., 2011). This study suggests the activation of 1/2<111> and <100> dislocations and the importance of dislocation climb at P, T conditions of the TZ because of the lack of slip planes and the development of sub-grain boundaries. Other experimental work on silicate garnet (Cordier et al., 1996; Voegelé et al., 1998a,b) and shock veins (Voegelé et al., 2000) supports the main conclusions of Couvy et al. (2011) through observations of the formation of large-scale dislocation junctions and sub-grain boundaries as typical in-

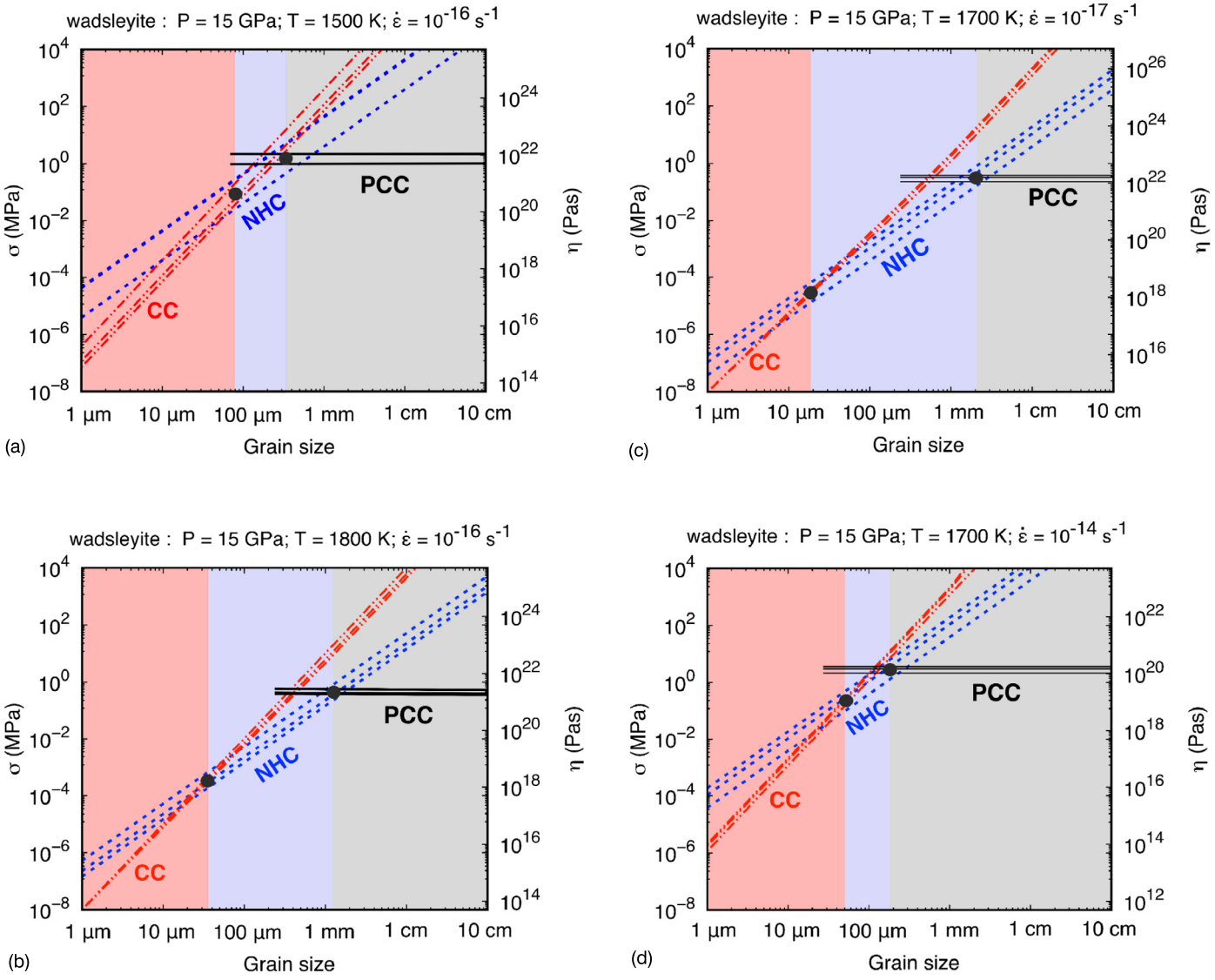

Fig. 3. Deformation mechanism maps of wadsleyite at 15 GPa, comparing Coble creep (CC), Nabarro-Herring creep (NH) and pure climb creep (PCC). a) Corresponds to a strain rate $\dot{\varepsilon}$ of 10^{-16} s^{-1} with T between 1500 K and b) 1800 K, respectively. c) Corresponds to $T = 1700$ K with $\dot{\varepsilon}$ between 10^{-17} s^{-1} and d) 10^{-14} s^{-1}, respectively.

dications for enhanced dislocation climb. All these studies support the inefficiency of dislocation glide as a result of high lattice friction opposed to dislocation glide in majorite garnet. Moreover, not only lattice friction appears to be comparably large in majorite garnet and the high-P polymorphs of olivine, but also their self-diffusivities are found to be similar (Fig. 1). This agrees well with a high viscous strength of majorite, equal to that of wadsleyite and ringwoodite under experimental conditions, as suggested by previous studies (Karato et al., 1995; Kavner et al., 2000), in contrast to the results of Hunt et al. (2010) arguing that majorite might be the weakest phase in the TZ, relying on stress relaxation experiments. Most previous studies however provide evidence that the plasticity of majorite garnet at TZ conditions is similar to that of wadsleyite and ringwoodite where dislocation creep operates in the PCC regime. Based on this hypothesis, we construct deformation mechanism maps of majorite garnet, including NHC and PCC based on self-diffusion experiments (van Mierlo et al., 2013), in analogy to wadsleyite and ringwoodite. Coble creep is not considered because of the lack of data. The Ω at TZ P, T conditions is taken from Wentzcovitch et al. (2010), μ is estimated as the depth-weighted average from PREM (Dziewonski and Anderson, 1981) and b of the 1/2<111> dislocation (Couvy et al., 2011) is considered. The deformation mechanism maps of majorite garnet at 18 GPa are shown in Fig. 5 for strain rates between 10^{-14} and 10^{-17} s^{-1} and T between 1600-2000 K. PCC is dominant when grains are larger than ~0.3-3 mm, below which diffusion creep becomes more efficient. A maximum viscosity of 10^{22} Pa.s is found in agreement with deformation mechanism maps of wadsleyite and ringwoodite.

4. Discussion

The theoretical predictions of the viscosity of wadsleyite, ringwoodite and majorite garnet (Figs. 3, 4 and 5) deforming by PCC are shown to be very similar with values of $10^{21\pm1}$ Pa.s corresponding to grains larger than ~0.1-1 mm at stresses of ~0.1-10 MPa and TZ P, T and $\dot{\varepsilon}$ conditions. This agrees remarkably well with the relatively constant viscosity of $\sim 10^{21}$ Pa.s predicted for the bulk TZ from global inversion of geodetic observations (Mitrovica and Forte, 2004). This supports that PCC is able to govern the deformation of polycrystalline wadsleyite, ringwoodite and majorite garnet with grains of at least ~0.1-1 mm or larger. Currently, deformation experiments (e.g. Nishihara et al., 2008; Farla et al., 2015; Hustoft et al., 2013; Kawazoe et al., 2010; Nishiyama et al., 2005; Miyagi et al., 2014) are not yet able to handle sufficiently

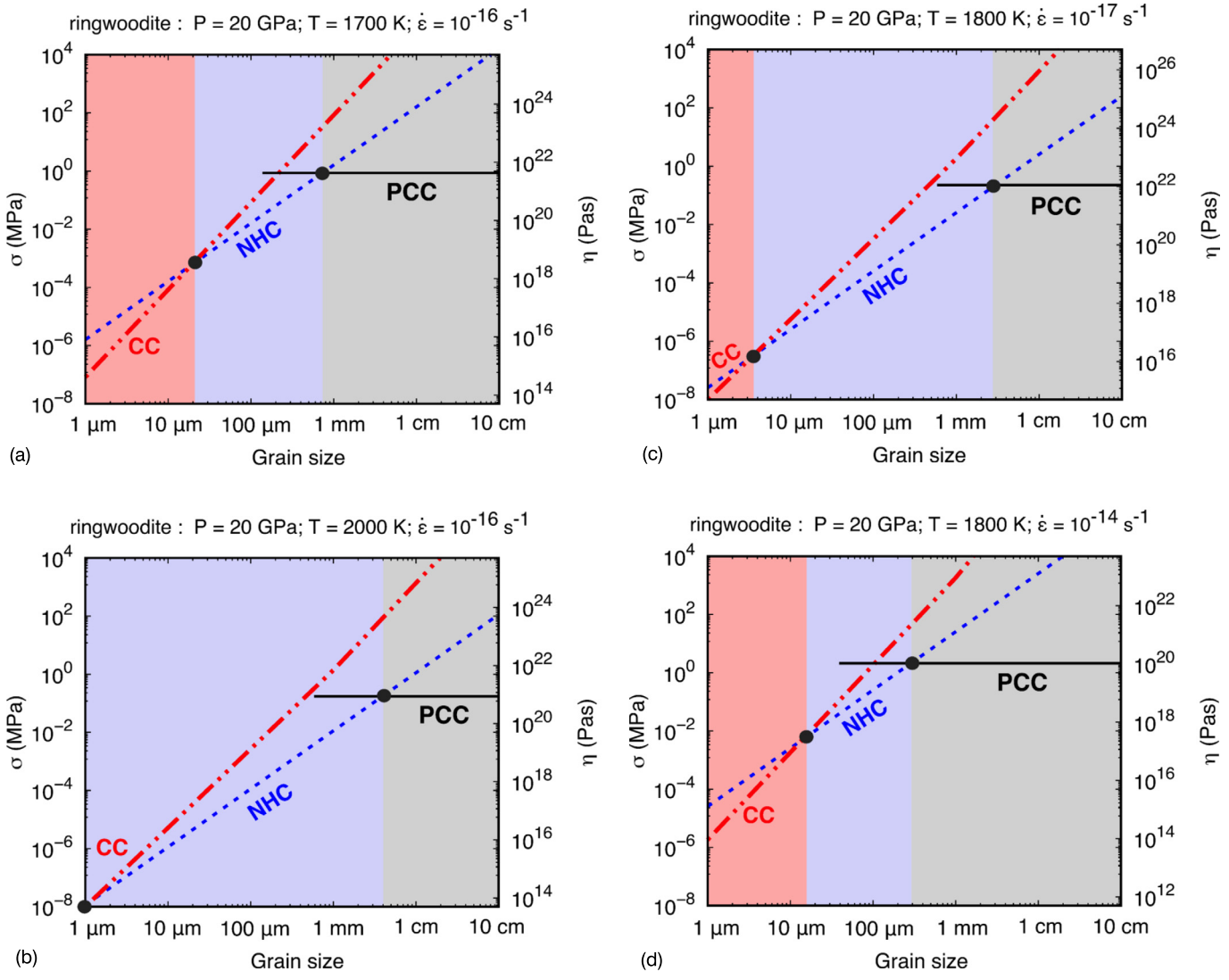

Fig. 4. Deformation mechanism maps of ringwoodite at 20 GPa, comparing Coble creep (CC), Nabarro-Herring creep (NH) and pure climb creep (PCC). a) Corresponds to a strain rate $\dot{\varepsilon}$ of 10^{-16} s^{-1} with T between 1700 K and b) 2000 K, respectively. c) Correspond to $T = 1800$ K with $\dot{\varepsilon}$ between 10^{-17} s^{-1} and d) 10^{-14} s^{-1}, respectively.

low stresses and strain rates (Fig. 2) to evidence the transition from the Weertman type of dislocation creep to pure climb creep. At the appropriate stress and strain rate conditions expected in the mantle, our modeling approach predicts that the pure climb creep mechanism might play an important role in the intracrystalline plasticity of the TZ. Glišović et al. (2015) inferred the grain size distribution across the Earth's mantle from inversion of geodetic observations in conjunction with considerations of grain growth and under the assumption that the mantle deforms by bulk diffusion creep. Their results show a grain size variation across the TZ between ∼0.4-2.4 mm. On the contrary, our modeling results provide evidence that wadsleyite, ringwoodite and majorite garnet grains of ∼0.4-2.4 mm are able to deform by PCC under the P, T conditions of the TZ (Figs. 3–5). This inconsistency suggests that the grain size distribution across the TZ might not be appropriately predicted based on the approach of Glišović et al. (2015). However, deformation of grains smaller than ∼0.1 mm would shift the dominant deformation mechanism to the pure diffusion creep regime leading to underestimated values of the viscosity with respect to geophysical observations. Some of the geodetic inversion profiles (Mitrovica and Forte, 2004; Rudolph et al., 2015) although, predict a local decrease in viscosity to $\sim 10^{-19}$ Pa.s at the base of TZ, starting just above ∼670 km. This region is characterized by the decomposition of ringwoodite and majorite garnet into bridgmanite and ferropericlase where grain size reduction might be expected. It can be seen in Figs. 4 and 5 that grains of ∼0.01-0.1 mm have a viscosity $\sim 10^{-19}$ Pa.s where deformation of ringwoodite and majorite garnet would be predominantly governed by NHC. This implies that a potential weak interface between the TZ and lower mantle does not require the presence of melt nor hydrolytic weakening. Indeed, experimental results suggested that grain size reduction might accompany phase transformations in the TZ (Rosa et al., 2016), providing evidence for small grains in both downwelling slabs (Kerschhofer et al., 1996) and upwelling plumes (Dobson and Mariani, 2014) across the 410 and 660 km discontinuity, respectively. Other experimental results however suggest grain growth to occur during the olivine to wadsleyite phase transition under shear stress across the 410 km discontinuity (Demouchy et al., 2011). Generally, the present deformation mechanism maps predict that diffusion creep becomes dominant in grains smaller than ∼0.1 mm, where a viscosity reduction with respect to PCC can be expected.

Not only phase transitions but also temperature variations might affect grain size in the TZ because of the presence of cold slabs and hot plumes. Although it is the interplay between many parameters (e.g. presence of trace elements, impurities and defor-

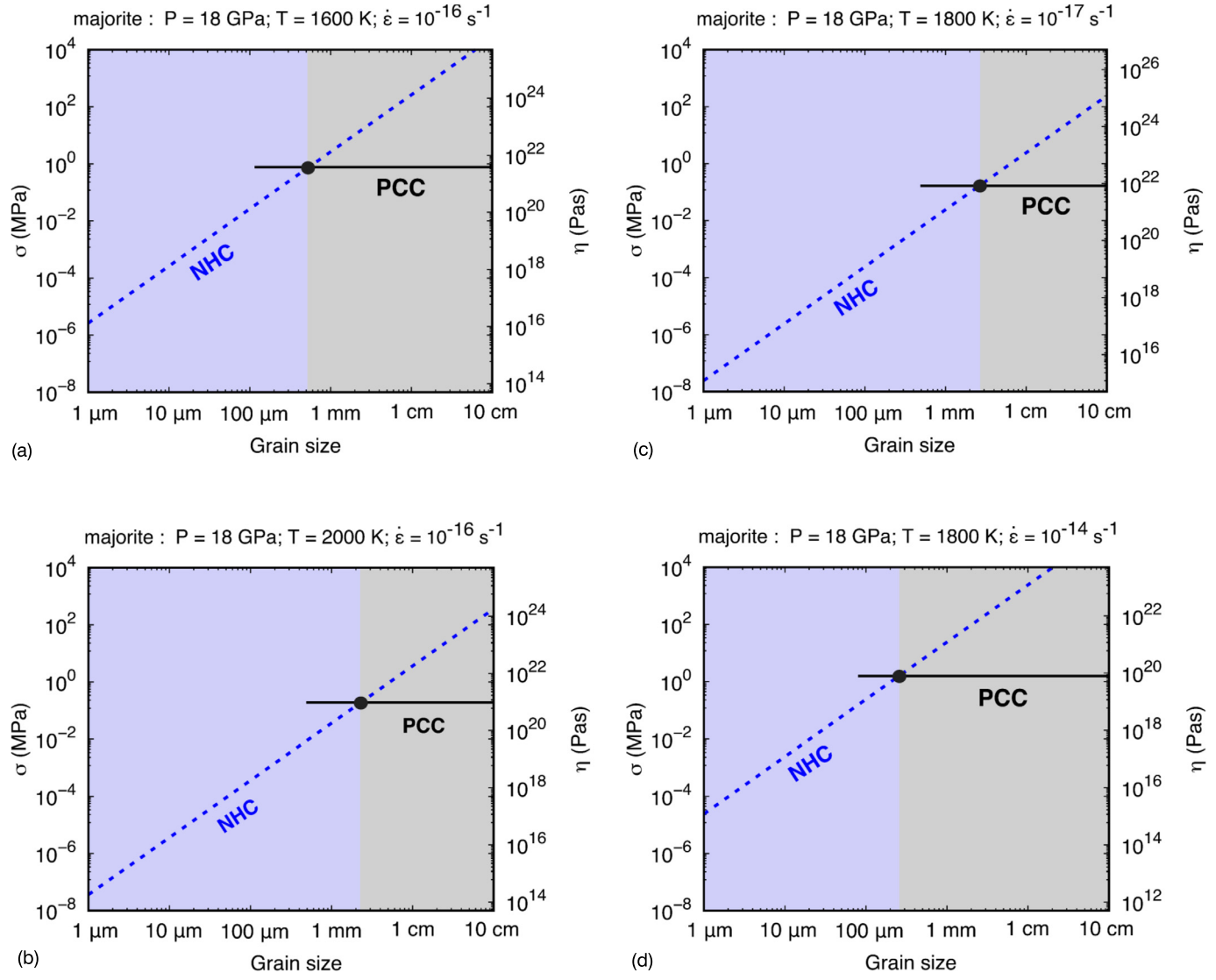

Fig. 5. Deformation mechanism maps for majorite garnet at 18 GPa, comparing Nabarro-Herring creep (NH) and pure climb creep (PCC). a) Corresponds to a strain rate $\dot{\varepsilon}$ of 10^{-16} s^{-1} with T between 1600 K and b) 2000 K, respectively. c) Correspond to $T = 1800$ K with $\dot{\varepsilon}$ between 10^{-17} s^{-1} and d) 10^{-14} s^{-1}, respectively.

mation history) which determines the average grain size, increasing temperature is generally expected to promote grain growth, suggesting that grains in plumes may tend to be larger than in the rest of the mantle, whereas they might be smaller in subducting slabs (e.g. Solomatov, 1996; Karato et al., 2001; Solomatov et al., 2002). Under this assumption, plumes are expected to deform by the same mechanism when PCC controls deformation of the surrounding bulk TZ. Cold slabs with smaller grains however might induce a change in deformation mechanism. Our results predict that diffusion creep becomes dominant in the TZ minerals when grain size drops below 0.1-1 mm accompanied by a decreasing viscosity. These results are in good agreement with Shimojuku et al. (2004), showing that the viscosity of wadsleyite can be explained by diffusion creep of grains of ∼0.5-5 mm. Previous experiments (Yamazaki et al., 2005) estimated that ringwoodite grains in subducting slabs might be even less than ∼0.1 mm. This implies that ringwoodite would deform by NHC (Fig. 4 a and b), leading to a reduction of ∼3 orders of magnitude in viscous strength (∼10^{18} Pa.s) compared to the surrounding TZ deforming by PCC (∼10^{21} Pa.s) at 2000 K (Fig. 4b). However, subducting slabs are typically colder than the surrounding TZ. The deformation of ringwoodite grains (0.1 mm) by NHC at 1700 K (Fig. 4a) still result in a viscosity reduction of 1 order of magnitude (∼10^{20} Pa.s) compared to a surrounding TZ (∼10^{21} Pa.s) deforming by PCC at 2000 K (Fig. 4b). This suggests that colder subducting slabs are able to become less viscous than the hotter surrounding TZ, particularly when grains are smaller than 0.1 mm. It should be mentioned that a decrease in T leads to a reduction in the transition grain size from NHC to PCC and favors the activation of pure climb creep in smaller grains (Fig. 4). This tends to decrease the viscous contrast between cold slabs and the surrounding TZ. Nevertheless, our results predict that cold slabs ($\Delta T \sim 300$ K) might be locally weaker than the surrounding TZ and might be well able to accommodate slab deflection (Fukao and Obayashi, 2013) in the TZ. The latter agrees well with recent deformation experiments suggesting that significant weakening of slabs is possible when fine ringwoodite grains are deformed by diffusion creep (Mohiuddin et al., 2020).

Apart from subducting slabs, our study predicts that the bulk TZ should be approximately equiviscous if deformation occurs predominantly by PCC. Since PCC is grain size independent, this mechanism provides an upper viscosity limit, which is not expected to exceed 10^{22} Pa.s in the TZ. This value falls in the range of the theoretically predicted viscosity of bridgmanite (Reali et al., 2019). Therefore, no global viscosity jump across the TZ into the lower mantle can be expected if PCC contributes the overall plasticity of the TZ. Nevertheless, the TZ rheology is ultimately constrained by

self-diffusion in the framework of PCC accommodated deformation. Experimental data on self-diffusion in wadsleyite, ringwoodite and majorite garnet (Fig. 1 and Tables 1 and 2) do not show large variations. These data should however be treated with caution since diffusion experiments at high-P, T remain a challenging task. Indeed, the TZ might be chemically heterogeneous, particularly since wadsleyite and ringwoodite are capable in bearing a significant amount of H^+ (Smyth, 1987; Inoue et al., 1995; Smyth et al., 2003; Pearson et al., 2014), but also Fe^{3+} (McCammon et al., 2004). The latter might strongly depend on the local oxygen fugacity, affecting point defect concentrations and mobilities which control the PCC mechanism. Shimojuku et al. (2010) determined the effect of hydrogen and iron on the Si diffusivity in wadsleyite. Based on the analysis of point defect chemistry, they found a positive dependence of the Si diffusion coefficient and water concentration, suggesting self-diffusion in hydrous wadsleyite to occur by the vacancy mechanism. This is in agreement with previous theoretical studies suggesting that incorporation of H^+ in mantle silicates as forsterite (Brodholt, 1997) and bridgmanite (Ammann et al., 2010) tends to increase the concentration of Si vacancies and enhance self-diffusion. Nevertheless, Shimojuku et al. (2010) show that the Si diffusivity in wadsleyite with up to 507 wt. ppm H_2O is only half an order of magnitude faster than those with only up to 60 wt. ppm H_2O (Fig. 1). Indeed, experimental data of Si self-diffusivities in wadsleyite are very similar and do not show large variations (less than one order of magnitude) at P, T conditions of the TZ despite the variation in starting materials (Fig. 1). The associated variation in creep behavior is shown to be small in wadsleyite (Fig. 3). Moreover, a TZ deforming predominantly by PCC based on Si diffusion data agrees well with the predicted TZ viscosity from geodetic inversion studies. Therefore, no significant diffusion-related hydrolytic weakening is expected in the TZ since the Si diffusivities are not found to decrease by more than a factor $\sim$5 due the presence of hydrogen (Shimojuku et al., 2010), in contrast to what has been previously suggested based on dislocation creep in ringwoodite (Fei et al., 2017).

A TZ where both PCC and diffusion creep dominate its overall plasticity is expected to be rheologically distinct from the upper mantle where Weertman creep is expected to operate (Hirth and Kohlstedt, 2003; Demouchy et al., 2012; Boioli et al., 2015a,b). Whereas Weertman creep of elastically anisotropic minerals as olivine develops CPO, PCC does not. This is consistent with observations of a strong seismic anisotropy in the first $\sim$300 km of the upper mantle (e.g. Fischer and Wiens, 1996; Long and van der Hilst, 2006), decreasing with increasing depth and becoming comparably small throughout most of the TZ, except in the vicinity of subduction zones (Drilleau et al., 2013; Moulik and Ekström, 2014; Lynner and Long, 2015; Huang et al., 2019; Ferreira et al., 2019). Fig. 2 shows that increasing the mantle flow stress to $\sim$500 MPa and $\sim$1200 MPa in wadsleyite and ringwoodite respectively, causes the glide velocity of dislocations to become similar to that of climb, allowing the activation of Weertman creep. Mantle stresses are commonly considered to be $\sim$1-10 MPa on average. Increasing the mantle flow stress by $\sim$1-2 orders of magnitude would be sufficient to activate dislocation creep in wadsleyite, whereas a slightly larger increase by $\sim$2-3 orders of magnitude would be required for ringwoodite. Activation of dislocation creep in the elastically anisotropic wadsleyite and ringwoodite is expected to produce CPO (Mainprice, 2007). Because stress concentrations might be particularly induced around subduction zones, such as in corner flows around stagnating slabs, CPO might develop around subduction zones by the activation of Weertman creep, particularly in wadsleyite (Kawazoe et al., 2013; Chang and Ferreira, 2019). On the contrary, our results predict that mantle stresses of $\sim$1 MPa in the TZ would favor the activation of PCC in the dislocation creep regime, consistent with the relative seismic isotropy of the bulk TZ.

5. Conclusion

We derived deformation mechanism maps of wadsleyite, ringwoodite and majorite garnet at the P, T conditions of the TZ and mantle strain rates based on theoretical plasticity models without the need of extrapolation. In the dislocation creep regime, we demonstrate that strain is more efficiently produced by dislocation climb than by glide, activating the deformation mechanism of PCC. Plastic deformation of the TZ minerals by PCC with a grain size of $\sim$0.1-1 mm or larger leads to an equiviscous TZ of $10^{21\pm1}$ Pa.s, in good agreement with viscosity profiles from geodetic observations. Our results suggest no global viscosity jump across the TZ into the lower mantle. Moreover, pure climb creep does not produce CPO which can explain the relatively small degree of seismic anisotropy observed in the TZ compared to the upper mantle. Nevertheless, our model results also predict that increasing the mantle flow stress by $\sim$1-3 orders of magnitude promotes deformation of the high-P polymorphs of olivine, in particular wadsleyite, by Weertman creep, which is able to produce CPO. Because stress concentrations occur most likely along subducting slabs, CPO in the TZ is expected to develop particularly in the vicinity of subduction zones, in agreement with seismic observations. On the other hand, viscosity reductions can be expected if grains become smaller than $\sim$0.1 mm, such as in cold subducting slabs or across phase transitions, by the activation of diffusion creep mechanisms. This provides evidence that cold subducting slabs might be locally weaker than the hotter surrounding TZ.

Declaration of competing interest

The authors declare that they have no known competing financial interests or personal relationships that could have appeared to influence the work reported in this paper.

Acknowledgements

This work was supported by the European Research Council under the Seventh Framework Programme (FP 7), ERC [grant number 290424 RheoMan] and under the Horizon 2020 research and innovation programme [grant number 787198 TimeMan].

References

Ammann, M.W., Brodholt, J.P., Dobson, D.P., 2010. Simulating diffusion. Rev. Mineral. Geochem. 71, 201–224.
Bardeen, J., Herring, C., 1952. Diffusion in alloys and the Kirkendall effect. In: Schockley, W. (Ed.), Imperfections in Nearly Perfect Crystals. Wiley, New York.
Boioli, F., Tommasi, A., Cordier, P., Demouchy, S., Mussi, A., 2015a. Steady state and low stresses in lithospheric mantle inferred from dislocation modelling of creep in olivine. Earth Planet. Sci. Lett. 432, 232–242.
Boioli, F., Carrez, Ph., Cordier, P., Devincre, B., Marquille, M., 2015b. Modeling the creep properties of olivine by 2.5-D dislocation dynamics simulations. Phys. Rev. B 92, 014115.
Boioli, F., Carrez, P., Cordier, P., Devincre, B., Gouriet, K., Hirel, P., Kraych, A., Ritterbex, S., 2017. Pure climb creep mechanism drives flow in the Earth's lower mantle. Sci. Adv. 3, e1601958.
Brodholt, J., 1997. Ab initio calculations on point defects in forsterite (Mg_2SiO_4) and implications for diffusion creep. Am. Mineral. 82, 1049–1053.
Chang, S.-J., Ferreira, A.M.G., 2019. Interference on water content in the mantle transition zone near subducted slabs from anisotropy tomography. Geochem. Geophys. Geosyst. 20, 1189–1201.
Coble, R.L., 1963. A model for boundary-diffusion controlled creep in polycrystalline materials. J. Appl. Phys. 34, 1679–1683.
Cordier, P., Raterron, P., Wang, Y., 1996. TEM investigation of dislocation microstructure of experimentally deformed silicate garnet. Phys. Earth Planet. Inter. 97, 121–131.
Couvy, H., Cordier, P., Chen, J., 2011. Dislocation microstructures in majorite garnet experimentally deformed in the multi-anvil apparatus. Am. Mineral. 96, 549–552.
Danas, K., Deshpande, V.S., 2013. Plane-strain discrete dislocation plasticity with climb-assisted glide motion of dislocations. Model. Simul. Mater. Sci. Eng. 21, 045008.

Demouchy, S., Tomassi, A., Barou, F., Mainprice, D., Cordier, P., 2012. Deformation of olivine in torsion under hydrous conditions. Phys. Earth Planet. Inter. 202–203, 56–70.
Demouchy, S., Mainprice, D., Tommasi, A., Couvy, H., Barou, F., Frost, D.J., Cordier, P., 2011. Forsterite to wadsleyite phase transformation under shear stress and consequences for the Earth's mantle transition zone. Phys. Earth Planet. Inter. 184, 91–104.
Dobson, D.P., Mariani, E., 2014. The kinetics of the reaction of majorite plus ferropericlase to ringwoodite: implications for mantle upwellings crossing the 660 km discontinuity. Earth Planet. Sci. Lett. 408, 110–118.
Drilleau, M., Beucler, É., Mocquet, A., Verhoeven, O., Moebs, G., Burgos, G., Montagner, J.-P., Vacher, P., 2013. A Bayesian approach to infer radial models of temperature and anisotropy in the transition zone from surface wave dispersion curves. Geophys. J. Int. 195, 1165–1183.
Dziewonski, A.M., Anderson, D.L., 1981. Preliminary reference Earth model. Phys. Earth Planet. Inter. 25, 297–356.
Farla, R., Amulele, G., Girard, J., Miyajima, N., Karato, S.-I., 2015. High-pressure and high-temperature deformation experiments on polycrystalline wadsleyite using the rotational Drickamer apparatus. Phys. Chem. Miner. 42, 541–558.
Fei, H., Yamazaki, D., Sakurai, M., Miyajima, N., Ohfuji, H., Katsura, T., Yamamoto, T., 2017. A nearly water-saturated mantle transition zone inferred from mineral physics viscosity. Sci. Adv. 3, e1603024.
Ferreira, A.M.G., Faccenda, M., Sturgeon, W., Chang, S.-J., Schardong, L., 2019. Ubiquitous lower-mantle anisotropy beneath subduction zones. Nat. Geosci. 12, 301–306.
Fischer, K.M., Wiens, D.A., 1996. The depth distribution of Mantle Anisotropy beneath the Tonga Subduction Zone. Earth Planet. Sci. Lett. 142, 253–260.
French, S.W., Romanowicz, B., 2015. Broad plumes rooted at the base of the Earth's mantle beneath major hotspots. Nature 525, 95–99.
Fukao, Y., Widiyantoro, S., Obayashi, M., 2001. Stagnant slabs in the upper and lower mantle transition region. Rev. Geophys. 39, 291–323.
Fukao, Y., Obayashi, M., 2013. Subducted slabs stagnant above, penetrating through, and trapped below the 660 km discontinuity. J. Geophys. Res. 118, 5920–5938.
Glišović, P., Forte, A.M., Ammann, M.W., 2015. Variations in grain size and viscosity based on vacancy diffusion in minerals, seismic tomography, and geodynamically inferred mantle rheology. Geophys. Res. Lett. 42, 6278–6286.
Grand, S.P., 2002. Mantle shear-wave tomography and the fate of subducted slabs. Philos. Trans. 360, 2475–2491.
Herring, C., 1950. Diffusional viscosity of a polycrystalline solid. J. Appl. Phys. 21, 437.
Hirth, G., Kohlstedt, D.L., 2003. Rheology of the Upper Mantle and the Mantle Wedge: A View from Experimentalists. Geophysical Monograph Series, vol. 138, pp. 83–105.
Holzapfel, C., Chakraborty, S., Rubie, D.C., Frost, D.J., 2009. Fe-Mg interdiffusion in wadsleyite: the role of pressure, temperature and composition and the magnitude of jump in diffusion rates at 410 km discontinuity. Phys. Earth Planet. Inter. 172, 28–33.
Huang, M., Li, Z., Tong, J., 2014. The influence of dislocation climb on the mechanical behaviour of polycrystals and grain size effect at elevated temperature. Int. J. Plast. 61, 112–127.
Huang, Q., Scherr, N., Waszek, L., Beghein, C., 2019. Constraints on Seismic Anisotropy in the Mantle Transition Zone from long-period SS precursors. J. Geophys. Res. 124, 6779–6800.
Hunt, S.A., Dobson, D.P., Li, L., Weidner, D.J., Brodholt, J.P., 2010. Relative strength of the pyrope-majorite solid solution and the flow-law of majorite containing garnets. Phys. Earth Planet. Inter. 179, 87–95.
Hustoft, J., Amulele, G., Ando, J.-I., Otsuka, K., Du, Z., 2013. Plastic deformation experiments to high strain on mantle transition zone minerals wadsleyite and ringwoodite in the rotational Drickamer apparatus. Earth Planet. Sci. Lett. 361, 7–15.
Inoue, T., Yurimotot, H., Kudoh, Y., 1995. Hydrous modified spinel, $Mg_{1.75}SiH_{0.5}O_4$: a new water reservoir in the mantle transition region. Geophys. Res. Lett. 22, 117–120.
Ita, J., Stixrude, L., 1992. Petrology, elasticity, and composition of the Mantle Transition Zone. J. Geophys. Res. 97, 6849–6866.
Karato, S.-I., Wang, Z., Liu, B., Fujino, K., 1995. Plastic deformation of garnets: systematics and implications for the rheology of the mantle transition zone. Earth Planet. Sci. Lett. 130, 13–30.
Karato, S.-I., Riedel, M.R., Yuen, D.A., 2001. Rheological structure and deformation of subducted slabs in the mantle transition zone: implications for mantle circulation and deep earthquakes. Phys. Earth Planet. Inter. 127, 83–108.
Karato, S.-I., Jung, H., Katayama, I., Skemer, P., 2008. Geodynamic significance of Seismic Anisotropy of the Upper Mantle: new insights from laboratory studies. Annu. Rev. Earth Planet. Sci. 36, 59–95.
Kavner, A., Duffy, T.S., 2001. Strength and elasticity of ringwoodite at upper mantle pressures. Geophys. Res. Lett. 28, 2691–2694.
Kavner, A., Sinogeikin, S.V., Jeanloz, R., Bass, J.D., 2000. Equation of state and strength of natural majorite. J. Geophys. Res. 105, 5963–5971.
Kawazoe, T., Karato, S.-I., Ando, J., Jing, Z., Otsuka, K., Hustoft, J.W., 2010. Shear deformation of polycrystalline wadsleyite up to 2100 K at 14-17 GPa using a rotational Drickamer apparatus (RDA). J. Geophys. Res. 115, B08208.
Kawazoe, T., Ohuchi, T., Nishihara, Y., Nishiyama, N., Fujino, K., Irifune, T., 2013. Seismic anisotropy in the mantle transition zone induced by shear deformation of wadsleyite. Phys. Earth Planet. Inter. 216, 91–98.
Keralavarma, S.M., Cagin, T., Arsenlis, A., Benzerga, A.A., 2012. Power-law creep from discrete dislocation dynamics. Phys. Rev. Lett. 109, 265504.
Kerschhofer, L., Sharp, T.G., Rubie, D.C., 1996. Intracrystalline transformation of Olivine to Wadsleyite and Ringwoodite under Subduction Zone conditions. Science 274, 79–81.
Knight, D.T., Burton, B., 1989. The climb behaviour of a dislocation which is pinned at two points. Philos. Mag. 59, 1027–1044.
Long, M.D., van der Hilst, R.D., 2006. Shear wave splitting from local events beneath the Ryukyu arc: trench-parallel anisotropy in the mantle wedge. Phys. Earth Planet. Inter. 155, 300–312.
Lynner, C., Long, M.D., 2015. Heterogeneous seismic anisotropy in the transition zone and uppermost lower mantle: evidence from South America, Izu-Bonin and Japan. Geophys. J. Int. 201, 1545–1552.
Mainprice, D., 2007. Seismic anisotropy of the Deep Earth from a mineral and rock physics perspective. In: Schubert, G., Price, G.D. (Eds.), Treatise in Geophysics – Volume 2: Mineral Physics. Elsevier, Oxford, UK.
Martin, J.L., Caillard, D., 2003. Thermally Activated Mechanisms in Crystal Plasticity. Pergamon, New York.
McCammon, C.A., Frost, D.J., Smyth, J.R., Laustsen, H.M.S., Kawamoto, T., Ross, N.L., van Aken, P.A., 2004. Oxidation state of iron in hydrous mantle phases: implications for subduction and mantle oxygen fugacity. Phys. Earth Planet. Inter. 143–144, 157–169.
Meade, C., Jeanloz, R., 1990. The strength of mantle silicates at high pressure and room temperature: implications for the viscosity of the mantle. Nature 348, 533–535.
Mitrovica, J.X., Forte, A.M., 2004. A new inference of mantle viscosity based upon joint inversion of convection and glacial isostatic adjustment data. Earth Planet. Sci. Lett. 225, 177–189.
Miyagi, L., Amulele, G., Otsuka, K., Du, Z., Farla, R., Karato, S.-I., 2014. Plastic anisotropy and slip systems in ringwoodite deformed to high shear strain in the Rotational Drickamer Apparatus. Phys. Earth Planet. Inter. 228, 244–253.
Mohiuddin, A., Karato, S.-I., Girard, J., 2020. Slab weakening during the olivine to ringwoodite transition in the mantle. Nat. Geosci. 13, 170–174.
Mordehai, D., Clouet, E., Fivel, M., Verdier, M., 2008. Introducing dislocation climb by bulk diffusion in discrete dislocation dynamics. Philos. Mag. 88, 899–925.
Moulik, P., Ekström, G., 2014. An anisotropic shear velocity model of the Earth's mantle using normal modes, body waves, surface waves and long-period waveforms. Geophys. J. Int. 199, 1713–1738.
Nabarro, F.R.N., 1948. Report of a Conference on Strength of Solids. Phys. Soc. London, pp. 75–90.
Nabarro, F.R.N., 1967. Steady-state diffusional creep. Philos. Mag. 16, 231–237.
Nishihara, Y., Tinker, D., Kawazoe, T., Xu, Y., Jing, Z., Matsukage, K.N., Karato, S.-I., 2008. Plastic deformation of wadsleyite and olivine at high-pressure and high-temperature using a rotational Drickamer apparatus (RDA). Phys. Earth Planet. Inter. 170, 156–169.
Nishiyama, N., Wang, Y., Uchida, T., Irifune, T., Rivers, M.L., Sutton, S.R., 2005. Pressure and strain dependence of the strength of sintered polycrystalline Mg_2SiO_4 ringwoodite. Geophys. Res. Lett. 32, L04307.
Nzogang, B.C., Thilliez, S., Mussi, A., Kawazoe, T., Miyajima, N., Bouquerel, J., Cordier, P., 2018. Application of scanning precession electron diffraction in the transmission electron microscope to the characterization of deformation in wadsleyite and ringwoodite. Minerals 8, 153.
Pearson, D.G., Brenker, F.E., Nestola, F., McNeil, J., Nasdala, L., Hutchison, M.T., Matveev, S., Mather, K., Silversmit, G., Schmitz, S., Vekemans, B., Vincze, L., 2014. Hydrous mantle transition zone indicated by ringwoodite included within diamond. Nature 507, 221–224.
Poirier, J.P., 1985. Creep of Crystals. Cambridge University Press.
Reali, R., van Orman, J., Pigott, J., Jackson, J.M., Boioli, F., Carrez, P., Cordier, P., 2019. The role of diffusion-driven pure climb creep on the rheology of bridgmanite under lower mantle conditions. Sci. Rep. 9. 2053.
Ringwood, A.E., 1975. Composition and Petrology of the Earth's Mantle. McGraw-Hill, New York.
Ritterbex, S., Carrez, Ph., Gouriet, K., Cordier, P., 2015. Modeling dislocation glide in Mg_2SiO_4 ringwoodite: towards rheology under transition zone conditions. Phys. Earth Planet. Inter. 248, 20–29.
Ritterbex, S., Carrez, Ph., Cordier, P., 2016. Modeling dislocation glide and lattice friction in Mg_2SiO_4 wadsleyite in conditions of the Earth's transition zone. Am. Mineral. 101, 2085–2094.
Rosa, A.D., Hilairet, N., Ghosh, S., Perrillat, J.-Ph., Garbarino, G., Merkel, S., 2016. Evolution of grain sizes and orientations during phase transitions in hydrous Mg_2SiO_4. J. Geophys. Res., Solid Earth 121, JB013360.
Rudolph, M.L., Lekić, V., Lithgow-Bertelloni, C., 2015. Viscosity jump in Earth's mid-mantle. Nature 350, 1349–1352.
Shimojuku, A., Kubo, T., Ohtani, E., Yurimoto, H., 2004. Silicon self-diffusion in wadsleyite: implications for the rheology of the mantle transition zone and subducting plates. Geophys. Res. Lett. 31, L13606.

Shimojuku, A., Kubto, T., Ohtani, E., Nakamura, T., Okazaki, R., Dohmen, R., Chakraborty, S., 2009. Si and O diffusion in $(Mg, Fe)_2SiO_4$ wadsleyite and ringwoodite and its implications for the rheology of the mantle transition zone. Earth Planet. Sci. Lett. 284, 103–112.

Shimojuku, A., Kubo, T., Ohtani, E., Nakamura, T., Okazaki, R., 2010. Effects of hydrogen and iron on the silicon diffusivity of wadsleyite. Phys. Earth Planet. Inter. 183, 175–182.

Smyth, J.R., 1987. β-Mg_2SiO_4: a potential host for water in the mantle? Am. Mineral. 72, 1051–1055.

Smyth, J.R., Holl, C.M., Frost, D.J., Jacobsen, S.D., Langenhorst, F., McCammon, C.A., 2003. Structural systematics of hydrous ringwoodite and water in the Earth's interior. Am. Mineral. 88, 1402–1407.

Solomatov, V.S., 1996. Can hotter mantle have a larger viscosity? Geophys. Res. Lett. 23, 937–940.

Solomatov, V., El-Khozondar, R., Tikare, V., 2002. Grain size in the lower mantle: constraints from numerical modelling of grain growth in two-phase systems. Phys. Earth Planet. Inter. 129, 265–282.

van der Hilst, R.D., Engdahl, R., Spakman, W., Nolet, G., 1991. Tomographic imaging of subducted lithosphere below northwest Pacific island arcs. Nature 386, 578–584.

van Mierlo, W.L., Langenhorst, F., Frost, D.J., Rubie, D.C., 2013. Stagnation of subducting slabs in the transition zone due to slow diffusion in majorite garnet. Nat. Geosci. 6, 400–403.

Voegelé, V., Cordier, P., Langenhorst, F., Heinemann, S., 2000. Dislocations in meteoritic and synthetic majorite garnet. Eur. J. Mineral. 12, 695–702.

Voegelé, V., Ando, J.I., Cordier, P., Liebermann, R.C., 1998a. Plastic deformation of silicate garnets, I: high-pressure experiments. Phys. Earth Planet. Inter. 108, 305–318.

Voegelé, V., Cordier, P., Sautter, V., Sharp, T.G., Lardeaux, J.M., Marques, F.O., 1998b. Plastic deformation of silicate garnets, II: deformation microstructures in natural samples. Phys. Earth Planet. Inter. 108, 319–338.

Weertman, J., 1957. Steady-state creep through dislocation climb. J. Appl. Phys. 28, 362–364.

Wentzcovitch, R.M., Yu, Y.G., Wu, Z., 2010. Thermodynamic properties and phase relations in Mantle minerals investigated by first principles quasiharmonic theory. Rev. Mineral. Geochem. 71, 59–98.

Yamazaki, D., Inoue, T., Okamoto, M., Irifune, T., 2005. Grain growth kinetics of ringwoodite and its implications for rheology of the subducting slab. Earth Planet. Sci. Lett. 236, 871–881.

Yu, Y.G., Wentzcovitch, R.M., Vinograd, V.L., Angel, R.J., 2011. Thermodynamic properties of $MgSiO_3$ majorite and phase transitions near 660 km depth in $MgSiO_3$ and Mg_2SiO_4: a first principles study. J. Geophys. Res. 116, B02208.

Zhang, B., Wu, X., Zhou, R., 2011. Calculation of oxygen self-diffusion coefficients in Mg_2SiO_4 polymorphs and $MgSiO_3$ perovskite based on the compensation law. Solid State Ion. 186, 20–28.

Zhao, D., 2004. Global tomographic images of mantle plumes and subducting slabs: insight into deep Earth dynamics. Phys. Earth Planet. Inter. 146, 3–34.